Mechanistic Investigation into the Selective Anticancer Cytotoxicity and Immune System Response of Surface-Functionalised, Dichloroacetate-Loaded, UiO-66 Nanoparticles

Isabel Abánades Lázaro,[1] Salame Haddad,[2] José M. Rodrigo-Muñoz,[3] Claudia Orellana-Tavra,[2] Victoria del Pozo*[3] David Fairen-Jimenez*[2] and Ross S. Forgan*[1]

1. WestCHEM School of Chemistry, University of Glasgow, Joseph Black Building, University Avenue, Glasgow G12 8QQ, UK.
Email: ross.forgan@glasgow.ac.uk

2. Adsorption & Advanced Materials Laboratory, Department of Chemical Engineering & Biotechnology, University of Cambridge, Pembroke Street, Cambridge CB2 3RA, UK
Email: df334@cambridge.ac.uk

3. Department of Immunology, Instituto de Investigación Sanitaria Fundación Jiménez Díaz, Universidad Autónoma de Madrid (IIS-FJD, UAM), and CIBER de Enfermedades Respiratorias (CIBERES) Madrid, Spain.
Email: VPozo@fjd.es

Keywords: metal-organic frameworks; drug delivery; surface modification; coordination modulation; endocytosis pathways; immune system response.

ABSTRACT

The high drug loading and excellent biocompatibilities of metal-organic frameworks (MOFs) have led to their application as drug delivery systems (DDSs). Nanoparticle surface chemistry dominates both biostability and dispersion of DDSs while governing their interactions with biological systems, cellular and/or tissue targeting, and cellular internalisation, leading to a requirement for versatile and reproducible surface functionalisation protocols. Herein, we explore not only the effect of introducing different surface functionality to the biocompatible Zr-MOF UiO-66, but also the efficacy of three surface modification protocols: (i) direct attachment of biomolecules (folic acid, biotin) introduced as modulators of UiO-66 synthetic, (ii) our previously reported ‘’click-modulation” approach to covalently attach polymers (poly(ethylene glycol), poly-L-lactide, poly-*N*-isopropylacrylamide) to the surface of UiO-66 through click chemistry, and (iii) surface ligand exchange, to postsynthetically coordinate folic acid, biotin and heparin to UiO-66. The innovative use of a small molecule with metabolic anticancer activity, dichloroacetic acid (DCA), as a modulator during synthesis is described, and found to be compatible with all three protocols, yielding surface-coated, DCA-loaded (10-20% *w/w*) nanoMOFs (70-170 nm).

External surface modification generally enhances stability and colloidal dispersion of UiO-66. Cellular internalisation routes and efficiencies of UiO-66 by HeLa cervical cancer cells can be tuned by surface chemistry, and anticancer cytotoxicity of DCA-loaded MOFs correlates with endocytosis efficiency and mechanisms. The MOFs with the most promising coatings (folic acid, poly(ethylene glycol), poly-L-lactide, and poly-*N*-isopropylacrylamide) were extensively tested for selectivity of anticancer cytotoxicity against MCF-7 breast cancer cells and HEK293 healthy kidney cells, as well as for cell proliferation and ROS production against J774 macrophages and peripheral blood lymphocytes (PBLs) isolated from the blood of human donors. DCA-loaded, folic acid modified UiO-66 selectively kills cancer cells without harming healthy ones or provoking immune system response *in vitro*, suggesting a significant targeting effect and great potential in anticancer drug delivery. The results provide mechanistic insight into the design and functionalisation of MOFs for drug delivery, and underline the availability of various *in vitro* techniques to potentially minimise early-stage *in vivo* animal studies, following the three Rs: reduction, refinement and replacement.

INTRODUCTION

Drug delivery systems (DDSs) have become an exciting alternative to conventional treatments for many diseases, such as cancer, as they have the potential to reduce unwanted side effects while maximizing treatment efficiency.[1] Several strategies have been studied, but the application of DDSs is often limited by bioavailability,[2] uncontrolled release of the drug (i.e. the burst effect),[3] poor loading capacity,[4] toxicity[5] and inefficient cellular internalisation.[6] Among them, metal-organic frameworks (MOFs)[7] – hybrid, highly porous crystalline structures composed of metal clusters linked by multidentate organic ligands – offer several advantages compared to available DDSs, as they combine desirable features of both organic (biocompatibility) and inorganic (high loadings) systems.[8-10]

Surface modifications of DDSs can minimize their interaction with the bulk, improving stability and dispersion,[11] and allowing them to cross physiological barriers,[12] providing the possibility of targeted carriers.[13] They can also decrease immune system recognition.[10,14] Despite the clear need to develop reproducible and versatile protocols to modify the outer surfaces of MOFs, few studies have addressed this issue so far, and even though it has been reported that drugs can be introduced into MOFs during synthesis,[15] achieving one pot-syntheses to create drug containing nanoparticulate MOFs (NMOFs) with functionalised surface is still a challenging goal. Different approaches to functionalise the surfaces of MOFs have been reported,[16] which can be categorised into functionalisation during synthesis, by using the coordination modulation approach,[17] or through postsynthetic modification.[18-20]

The Lewis acid character of MOFs' metal centres offers the possibility of coordinating nucleophiles to the coordinatively unsaturated metal sites available on the outer surface of NMOFs. In order to avoid inner surface functionalisation, this postsynthetic modification is usually achieved through size-selective protocols, where the functionality cannot penetrate the porosity. This approach was first reported by Rowe *et al.*,[18] and since then has been applied by different groups. For example, histidine residues (his-tags), which contain imidazole groups, have been used to coordinate several peptides and proteins to three different MOFs surfaces: to the copper benzenetricarboxylate MOF, HKUST-1; to the iron-fumarate MOF MIL-88A and to a related zirconium fumarate MOF.[19] Additionally, several polymer coatings, including oligonucleotides, have been added to the surfaces of MOFs by coordination to the metal clusters through one of the polymers' ends.[21-23] The well-known surface ligand exchange (SLE) protocol – postsynthetically exchanging surface ligands for desired functionality – is also based on coordination chemistry.[24]

It is also important to mention that silica coating has been widely used to increase MOFs' water stability, induce slow release, and to attach surface reagents through the siloxane

groups.[25] Although this approach can dramatically enhance some MOFs properties, drawbacks exist in the fact that the silica coating can block pore access, and that some silica nanoparticles have been found to be toxic.[26]

Postsynthetic covalent modifications, performed on functionalised organic linkers, have been widely used in biological applications of NMOFs.[27] For example, Lin and co-workers postsynthetically attached a cisplatin prodrug to MIL-101-NH_2 amino group present in the MOF linker[28] They also utilised a cisplatin prodrug as the linker directly during synthesis,[25] followed by silica coating and subsequent targeting peptide attachment. Once again, to selectively functionalise the outer surface, a surface reagent bigger than the pore opening is required. Additionally, unsaturated carboxylic acid groups present on the MOF surface can also be exploited for postsynthetic covalent surface modifications. For example, a green fluorescent protein was coupled to surface carboxylate groups of different MOFs using a carbodiimide-mediated reaction,[29] and then the protocol was applied to couple PEG5000-NH_2 and Stp-10C,[20] a derived oligoamino amide with proton-sponge features. However, the low reactivity of the organic linker's carboxylates hinders the application of this protocol, resulting in very low surface coatings (1-2% *w/w*).

Interest in zirconium-based MOFs as DDSs is arising as a consequence of their high chemical stability compared to iron MOFs,[30] and their safe use has been validated *in vitro*[12,23,31-39] and *in vivo*,[40] showing almost no acute cytotoxicity, with efficient performance in anticancer drug delivery. In particular, the zirconium terephthalate MOF UiO-66 (UiO standing for Universitetet i Oslo) has excellent biocompatibility[40] which, together with its well-known structure and characterisation,[41] ability to cross the cell membrane[33,36] and pH responsive drug release,[35,36] makes it a great candidate for nanoparticle-conjugated anticancer drug delivery. Additionally, it is well known that monocarboxylic acid functionalised modulators can be attached to its surface and defect sites during synthesis, yielding highly porous nanoparticles.[42]

We have previously reported the ''click modulation'' protocol for UiO-66,[32] in which we introduced functionalised modulators (*p*-azidomethylbenzoic acid, L1 and *p*-propargyloxybenzoic acid, L2, Fig 1) to UiO-66 nanoparticle surfaces and defect sites during their synthetic process, followed by postsynthetic covalent conjugation of different surface functionality using copper(I)-catalysed azide-alkyne cycloaddition (CuAAC). Attaching protecting PEG2000 chains to the MOF surface enhanced stability in phosphate buffered saline (PBS) solutions, enabled pH-responsive cargo release and tuned UiO-66 cell uptake pathways from clathrin-mediated to the more desirable caveolae-mediated route, which allows particles to circumvent cargo degradation in the lysosomes.[36] The effect of surface

chemistry on DDS efficiency was evident in the enhanced cytotoxicity of the anticancer drug, dichloroacetate (DCA), which can be loaded into the NMOF as a co-modulator (dichloroacetic acid) during synthesis. Only the PEGylated MOF enhanced the cytotoxicity of DCA towards HeLa cancer cells, likely as NMOFs internalised through caveolae-mediated endocytosis can escape the early endosome, resulting in cytosolic release of the cytotoxic cargo.

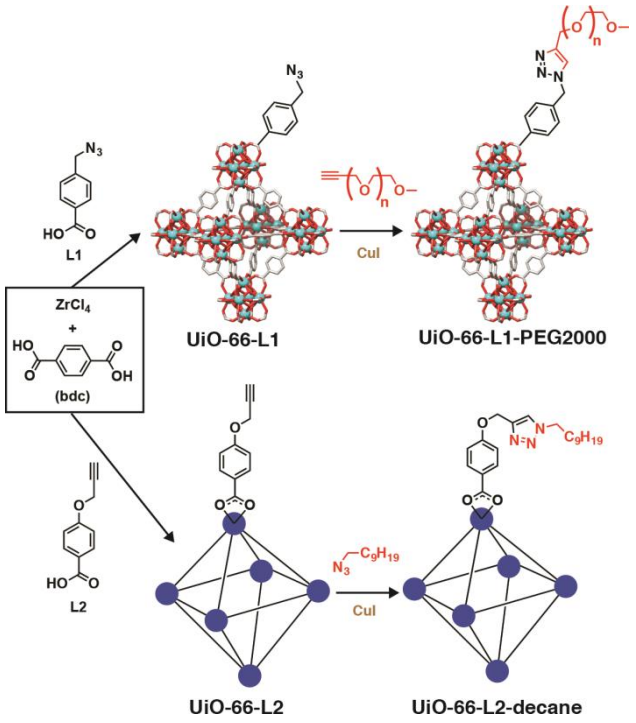

Figure 1. Schematic showing our "click modulation" surface functionalisation protocol for UiO-66 using the functionalised modulators L1 and L2.[32] Note that in this study, UiO-66-L2 is prepared by surface ligand exchange from UiO-66-L1, and not through coordination modulation.

The need to find a rationalisation between the intrinsic characteristics of NMOFs, such as surface chemistry, and their therapeutic efficacy is inherently clear, providing if so the possibility of reducing animal testing while maximizing the potential application of MOFs as DDSs. Thus, we chose to further explore the different ways of functionalising the outer surface of UiO-66 nanoparticles, in order to characterise the effect of surface modifications on properties such as physiological stability and colloidal dispersion. Then, through thoughtful choice of surface reagents with different characteristics – hydrophilic or hydrophobic, targeting agents, negatively charged, positively charged or neutral – we attempt to rationalise the effect of surface chemistry of UiO-66 on HeLa cell internalisation pathways, therapeutic efficiency, selectivity of cytotoxicity (targeting) and *in vitro* immune response.

RESULTS AND DISCUSSION

Three different surface modification protocols were assessed: (i) direct incorporation of functionality through coordination modulation (CM), (ii) postsynthetic surface ligand exchange (PS), and (iii) click modulation, wherein functionalised modulators are covalently modified (Figure 2a). Different surface reagents (Figure 2b) which possess various coordinating groups – vitamin B_9 folic acid (FA), vitamin B_7 biotin (Biot), and a negatively charged anticoagulant, heparin (Hep) – that are well known to play different biological roles in targeting and binding, were selected to be potentially coordinated to UiO-66 surfaces postsynthetically. The carboxylic acid functionalities of both folic acid and biotin allowed their direct incorporation during modulated syntheses. Additionally, the hydrophobic propargyl-terminated poly-L-lactide (PolyLact, M_n = 2000) and the hydrophilic azide-terminated poly-*N*-isopropylacrylamide (PNIPAM, M_n = 15000)[43] were selected as protecting polymers to click to UiO-66-L1 and UiO-66-L2 surface. Thus, we have evaluated the properties that different surface coatings provide to UiO-66 and the potential and reproducibility of different protocols to introduce different functionalities.

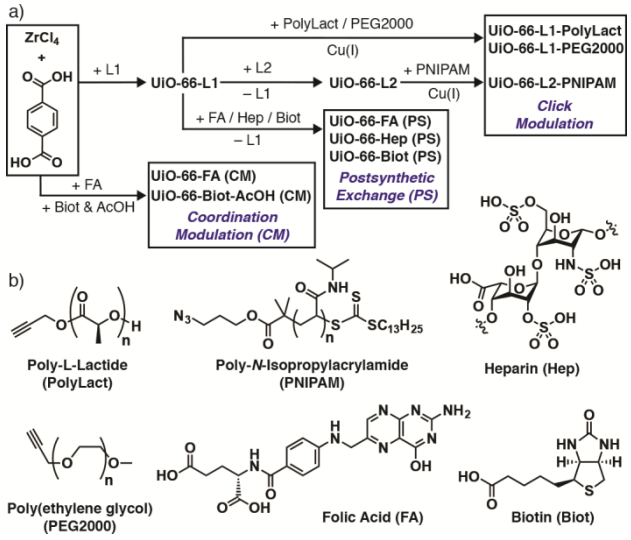

Figure 2. a) Synthetic scheme for the surface modified MOFs, highlighting 8 MOFs obtained through coordination modulation (CM), postsynthetic exchange (PS) and click modulation. b) Chemical structures of the surface functionality attached to the MOFs.

Synthesis and Characterisation

Coordination Modulation: UiO-66-L1 was synthesised (see Figure 2a for synthetic methodologies) following our previously reported coordination modulation solvothermal

protocol.[32] The coordination modulation approach, first reported by Fisher and co-workers,[44] is based on the use of modulators with similar chemical functionality to the linker during the synthetic process. However, the modulators can play different roles during synthesis, in some occasions inducing defects (such as missing linkers or clusters)[42] as well as capping crystal surfaces. This approach can also be used for size control[45] through coordination to the metal units (if acting as a capping agent) or through promotion of crystal growth. After successful synthesis of UiO-66-L1, L1 was replaced by L2 through surface ligand exchange, yielding UiO-66-L2, in order to maintain constant particle size. Full characterisation of both materials (SI, Section S3.1) showed highly crystalline nanoparticles, as confirmed by powder X-ray diffraction (PXRD), with the appropriate size for drug delivery, ca. 150 nm, determined by scanning electron microscopy (SEM), and high modulator content, determined by ^{1}H NMR spectroscopy (15-27 mol % compared to bdc). N_2 adsorption isotherms confirmed that L1 and L2 are attached to UiO-66 external surface and defect sites: S_{BET} = 1591 m^2g^{-1} (UiO-66-L1) and 1349 m^2g^{-1} (UiO-66-L2) are higher than pristine UiO-66, typically 1200 m^2g^{-1}.[41] These results show that L1 can be easily exchanged by L2 – and thus potentially other coordinating agents – postsynthetically on the outer surface of UiO-66-L1.

We subsequently used both folic acid and biotin as modulators in solvothermal syntheses of UiO-66 (SI, Section S3.2). The samples were named UiO-66-FA (CM) and UiO-66-Biot-AcOH (CM) to reflect that acetic acid was required as a co-modulator in the synthesis of the biotin-coated sample, where CM stands for coordination modulation to distinguish them from samples prepared by postsynthetic ligand exchange (Figure 2a). The samples were crystalline and phase pure as confirmed by PXRD (Figure 3a). ^{1}H NMR spectra of acid digested samples of the NMOFs showed the presence of the functional modulator in both cases (28 mol % for folate and only 2 mol % for biotin, see Table 1), but no AcOH in UiO-66-Biot-AcOH (CM). The gravimetric folic acid content was also calculated by UV-Vis spectroscopy of acid digested UiO-66-FA (CM), and found to be 13.6% (*w/w*)

Fourier transform infra-red (FT-IR) spectra showed appearance of modulator signals with slight shifts as a possible consequence of their coordination to the available zirconium units. In concordance, thermogravimetric analysis (TGA) profiles showed new mass loss events starting at higher temperatures than the free modulators' thermal decomposition, strongly indicating their attachment, which was unequivocally confirmed by nitrogen adsorption and desorption isotherms, revealing highly porous samples. UiO-66-Biot-AcOH (CM) was more porous – with a BET area of 1377 m^2g^{-1} – than UiO-66-FA (CM), which exhibited a BET area of 753 m^2g^{-1}. This could be explained by the higher modulator content in UiO-66-FA (CM) and the likely poorer crystallinity and/or smaller particle size indicated by the broad Bragg peaks in the PXRD pattern. SEM (Figure 3b) showed UiO-66-FA (CM) to have a

homogeneous distribution of small nanoparticles (~50 nm), reflected in the broadening of its PXRD pattern, and indicating that folic acid is acting as a capping agent during UiO-66 synthesis. On the other hand, UiO-66-Biot-AcOH (CM) forms as well-defined nanoparticles around 150 nm in size.

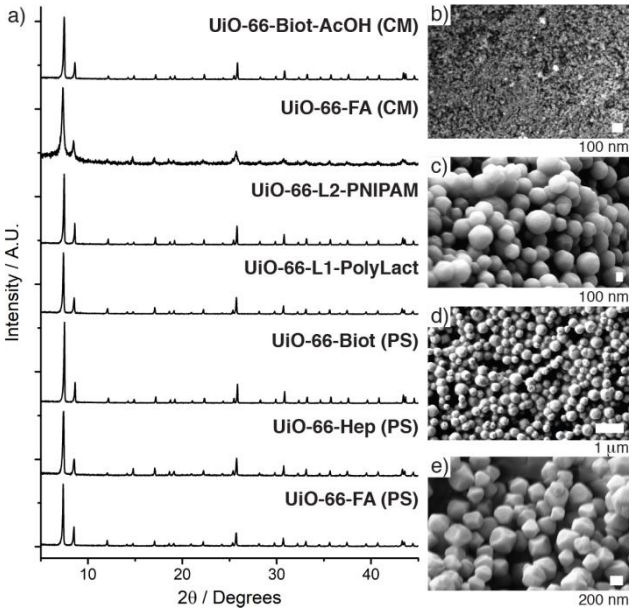

Figure 3. a) Stacked PXRD patterns of the surface modified UiO-66 samples. SEM images of b) UiO-66-FA (CM), showing a very small particle size consistent with the broad PXRD, c) UiO-66-L2-PNIPAM, showing a rounded morphology due to polymer coating, d) UiO-66-Biot (PS), and e) UiO-66-Biot-AcOH (CM), showing the differences in particle size and morphology from different surface modification techniques.

These results confirm that coordination modulation can be used to simultaneously control the surface chemistry and particle size of NMOFs. It has been previously reported that when the modulator is the only parameter varied during synthesis, particle size strongly correlates with the pK_a of the modulator.[45] Our results also suggest that pK_a influences modulator's attachment; the pK_a values of the carboxylic acids of bdc are 3.54 and 4.46, while folic acid has pK_a values of 3.5 and 4.3, biotin has a pK_a of 4.5, and AcOH a pK_a of 4.8, and therefore folic acid attachment is higher than biotin, while AcOH is not incorporated. Further, folic acid has two carboxylic acids in its structure while biotin has only one, and it has been reported that when coordinating histidine-conjugated peptides to a Zr-fumarate MOF, the binding affinity increases with the number of histidine residues.[19]

Table 1. Characterisation data for the surface-modified MOFs.

Sample	BET area (m^2g^{-1})	SEM Particle size (nm)	Estimated surface coating		
			^{1}H NMR (mol %)[a]	TGA (% *w/w*)[b]	UV-Vis (% *w/w*)[c]
UiO-66-L1	1591	143 ± 31	15	n/a	n/a
UiO-66-L2	1349	142 ± 14	27	n/a	n/a
UiO-66-L1-PolyLact	1129	177 ± 25	n/a	10	n/a
UiO-66-L2-PNIPAM	1030	177 ± 24	n/a	3	n/a
UiO-66-FA (PS)	879	168 ± 26	40	25	23.6
UiO-66-Biot (PS)	949	175 ± 17	10	12	n/a
UiO-66-Hep (PS)	891	157 ± 34	n/a	27	n/a
UiO-66-FA (CM)	753	36 ± 13	28	13	13.6
UiO-66-Biot-AcOH (CM)	1227	157 ± 16	2	4	n/a

[a]Values could not be measured for polymeric samples as integral ratios could not be accurately compared. [b]Values derived by TGA analysis are complicated by additional overlapping mass loss events and so should be considered estimates. [c]Only folic acid content can be determined by UV/Vis spectroscopy.

Surface Ligand Exchange: Postsynthetic coordination of folic acid, biotin and heparin to the surface of UiO-66-L1 was carried out, and the samples were named UiO-66-FA (PS), UiO-66-Biot (PS) and UiO-66-Hep (PS), where PS stands for postsynthetic (SI, Section 3.1). As a consequence of surface ligand exchange, D_2SO_4/d_6-DMSO acid-digested ^{1}H NMR spectra of the functionalised NMOFs showed disappearance of resonances for protons of L1 and appearance of resonances assigned to folic acid, biotin and heparin. FT-IR spectra of the MOFs showed the disappearance of the azide band of L1 and the appearance of new vibration bands characteristic of the surface reagents, some of them slightly shifted, possibly as a consequence of coordination. TGA profiles of the functionalised samples showed new mass loss events, starting at a higher temperature than authentic samples of the coordinating agents, strongly suggesting attachment by coordination rather than simply surface adhesion. The metal residue (ZrO_2) at 800 °C was considerably lower than for their precursor sample UiO-66-L1, suggesting significant organic mass addition at the surfaces. The fact that the samples retained porosity – with BET areas between 870 and 950 m^2g^{-1} – confirmed attachment to UiO-66 external surface without blocking the pores, although the

slightly lower gravimetric surface areas are likely a consequence of the additional mass of the surface functionality.

Click Modulation: Propargyl-terminated poly-L-lactide and azide-terminated poly-*N*-isopropylacrylamide were attached to UiO-66-L1 and UiO-66-L2 respectively by CuAAC "click" chemistry using our previously reported click-modulation protocol,[32] yielding UiO-66-L1-Poly-L-Lact and UiO-66-L2-PNIPAM nanoparticles (SI, Section 3.1). In a similar manner to our previously reported UiO-66-L1-PEG2000, the samples were fully characterised by TGA, FT-IR spectroscopy and N_2 adsorption isotherms, confirming the reproducibility of the click modulation protocol to covalently conjugate various polymers to UiO-66 outer surfaces. The TGA profile of UiO-66-L1-PolyLact showed new mass loss events (10% *w/w*) at a higher temperature than propargyl-terminated poly-L-lactide due to its covalent attachment. Similar features were observed in the TGA profile of UiO-66-L2-PNIPAM, for which we estimate a 3% (*w/w*) of PNIPAM present in the structure. The thermal stabilities of both functionalised NMOFs slightly decreased as a consequence of the thermal decomposition of the polymers anchored to their surface. Control samples, in which polymers were stirred with functionalised NMOFs without the presence of the Cu(I) catalyst, showed no new thermal decomposition steps or decrease in thermal stability, further indicating covalent attachment of the polymers using the CuAAC protocol. The physical changes to the surface functionalised NMOFs' morphologies were examined by SEM (Figure 3b), revealing a more rounded shape after surface coating compared to octahedral UiO-66-L1 nanoparticles, with the slight increase in particle size a consequence of the surface coating.

Stability and Dispersion of Surface Modified UiO-66

Our previous study showed that PEGylation enhanced the dispersion of UiO-66 in various solvents; unwanted aggregation could hinder cellular uptake and induce *in vivo* toxicity of DDSs.[32] The solution stability and aggregation of the surface-modified NMOFs were investigated through dynamic light scattering (DLS) measurements of samples dispersed (0.25 $mgml^{-1}$) in methanol, water and PBS (SI, Section S4). The postsynthetically functionalised samples were all derived from the same batch of UiO-66-L1, measured to be around 150 nm in size by SEM, allowing close comparison. In methanol, the highly charged heparin-coated UiO-66-Hep showed the greatest aggregation (ca. 700 nm) compared to UiO-66-L1 (ca. 300 nm), while the other samples showed less aggregation, particularly the polymer-modified UiO-66-L1-PolyLact and UiO-66-L2-PNIPAM samples (200-250 nm). Significant aggregation and precipitation of UiO-66-L1 and UiO-66-L2 were observed in water, and UiO-66-FA (PS) also formed significant aggregates (ca. 700 nm). UiO-66-Biot (PS) and UiO-66-L1-PolyLact showed a small degree of aggregation (ca. 400 nm) whilst

UiO-66-L2-PNIPAM was initially monodisperse (ca. 150 nm) but aggregated over time, and UiO-66-Hep appeared to shed its surface coating and precipitate, clearly indicating the effect of external surface modification on colloidal stability.

Measurements performed in PBS again showed aggregation and precipitation of UiO-66-L1 and UiO-66-L2, while after surface coating, more stable dispersions were found (Figure 4a). UiO-66-FA (PS), UiO-66-Biot (PS) and UiO-66-Hep (PS) all showed less aggregation than the uncoated samples, with stable dispersions of approximately 600-1000 nm. The samples covalently functionalised through the ‘‘click modulation’’ approach, UiO-66-L1-PolyLact and UiO-66-L2-PNIPAM, again had enhanced dispersive stability, with initial measurements showing size distributions close to those determined by SEM followed by slightly aggregation to 400-700 nm during the course of the experiment.

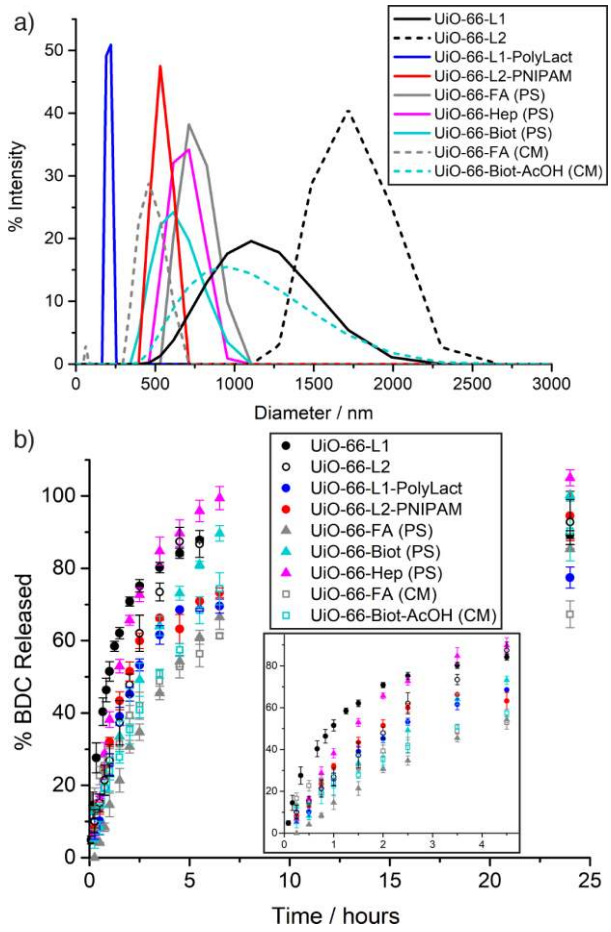

Figure 4. a) DLS measurements of the MOFs (0.25 mgml^{-1}, PBS) showing the effect of surface functionality on aggregation. b) Degradation profiles (release of bdc ligand in PBS), showing that surface groups can slow down degradation by phosphate.

Similar behaviour was observed for the samples functionalised through coordination modulation, UiO-66-FA (CM) and UiO-66-Biot-AcOH (CM), although the biotin-modified sample showed significant aggregation in PBS (ca. 1200 nm), possibly as a consequence of

its low (ca. 2 mol %) surface functionalisation. Overall, all the external surface modified samples showed enhanced dispersion in PBS compared to unmodified materials, with the extent of the improvement related to the size and charge of the surface functionality. It is important to note that while DLS measurements are performed without stirring, the blood current is a dynamic system. It has also been reported that while MOFs usually aggregate in PBS, the presence of proteins such as Bovine Serum Albumin (BSA), present in cells growth media and blood current, results in stable colloidal dispersions as a consequence of protein corona formation.[46] While the lability of the metal-linker bonds at acidic pH values ensures decomposition of NMOFs in intracellular conditions, thus avoiding accumulation in the body, the coordinative nature of this bond can be a disadvantage as coordinating groups, such as phosphates, are able to displace the linkers in extracellular conditions resulting in undesirable fast-release kinetics. External surface coatings[10] and approaches such as postsynthetic and post drug loading amorphisation[33,35] or silica coating[25] have been studied to overcome this problem. The stabilities of the externally surface coated NMOFs were determined in PBS (pH 7.4) by UV/Vis spectroscopic measurement of the release of the linker, bdc, and compared to the degradation profile of UiO-66-L1 (SI, Section S5). Additionally, the release of folic acid was determined for the corresponding two samples.

The postsynthetically external surface modified samples exhibit induction times of different lengths (1-4 h) depending on the sample, for which the degradation rates were considerably slower than UiO-66-L1 (Figure 4b). Interestingly, after 2.5 h, the degradation of UiO-66-Hep (PS) is higher than UiO-66-L1, showing that depending of the nature of the coating – in this case hydrophilic and highly soluble in water – the degradation rate can be also increased over certain timescales, if desired, by external surface modifications. In all the other cases, improvements in stability were found. Specifically, the UiO-66-L1 degradation profile (55% bdc release after 1 h) was tuned from exponential to sigmoidal in the case of UiO-66-L1-PolyLact (27% bdc release after 1 h) and UiO-66-L2-PNIPAM (30% release after 1 h). The effect of different functionalisation techniques (coordination modulation or postsynthetic) is apparent when analysing the degradation profiles of the biotin and folic acid modified samples. Although in all cases stability towards phosphates was clearly enhanced, UiO-66-FA (PS) and UiO-66-Biot (PS) exhibit a more pronounced induction time, with minor release during the first 30 minutes – both ~10% release versus 30% for UiO-66-L1, 15% for UiO-66-Biot-AcOH (CM) and 20% for UiO-66-FA (CM) – possibly due to a higher degree of pore blockage hindering phosphate attack at the first stages. However, after 1 h in the case of the biotin containing samples, and 4 h in the case of the folate containing samples, the percentage of bdc released is higher for the postsynthetically modified samples. These results are mirrored in the release of folate from the external surface of the MOFs.

Endocytosis Efficiencies and Routes of Surface-Modified UiO-66

Calcein was selected as a fluorescent molecule to track the NMOFs inside cells, in order to study endocytosis pathways.[33] Calcein's hydrophilicity does not allow it to efficiently cross the cell membrane, and thus intracellular cytoplasmic fluorescence is significantly increased when calcein is incorporated into a carrier.[36] UiO-66-L1 and UiO-66-L2 were postsynthetically loaded with calcein following previously reported protocols, and their surfaces subsequently modified either using our click modulation method[32] or postsynthetic external surface ligand exchange (PS) (Scheme 1), ensuring all samples were of similar particle size as they originated from one batch of UiO-66-L1.

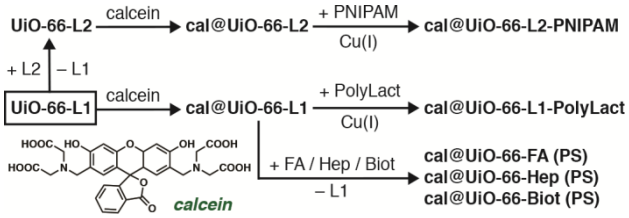

Scheme 1. Synthesis of calcein-loaded, surface modified MOFs obtained through postsynthetic exchange (PS) and click modulation.

cal@UiO-66-L1-PolyLact and cal@UiO-66-L2-PNIPAM were prepared through CuAAC mediated conjugation of the surface polymers, while cal@UiO-66-FA (PS), cal@UiO-66-Biot (PS), cal@UiO-66-Hep (PS) were prepared by external surface ligand exchange from cal@UiO-66-L1 to introduce the external surface moieties (SI, Section S6.1). As previously, full characterisation confirmed the surface moieties' attachment to the calcein-loaded NMOFs' surface, and calcein loading was measured by UV/Vis spectroscopy of digested samples (Table 2).

Table 2. Calcein loadings of the surface modified MOFs, determined by UV-Vis spectroscopy, and their subsequent endocytosis efficiencies for HeLa cells normalised to cal@UiO-66-L1.

Sample	Calcein Loading (UV-Vis, % *w/w*)	Endocytosis Efficiency %
cal@UiO-66-L1	17.9	100
cal@UiO-66-L1-PolyLact	6.9	141 ± 2
cal@UiO-66-L2-PNIPAM	8.0	150 ± 1
cal@UiO-66-FA (PS)	9.8	184 ± 2
cal@UiO-66-Hep (PS)	13.0	171 ± 3
cal@UiO-66-Biot (PS)	12.8	37 ± 1

Fluorescence-activated cell sorting (FACS) was used to study the endocytosis efficiencies and pathways of the calcein-loaded, external surface modified NMOFs when incubated with HeLa cervical cancer cells (SI, Section S6.2). As all the cal@NMOF samples were prepared from the same base batch, we assume that variations are caused by changes in external surface chemistry, not particle size, in concert with our previous work which shows particle size has only minor effect until sizes >500 nm are reached.[34] Uptake efficiency was analysed after incubating cells with a fixed NMOF concentration (0.5 mgmL^{-1}), normalising the data to UiO-66-L1 cell internalisation, taking into account differing calcein loading values (Figure 5a).

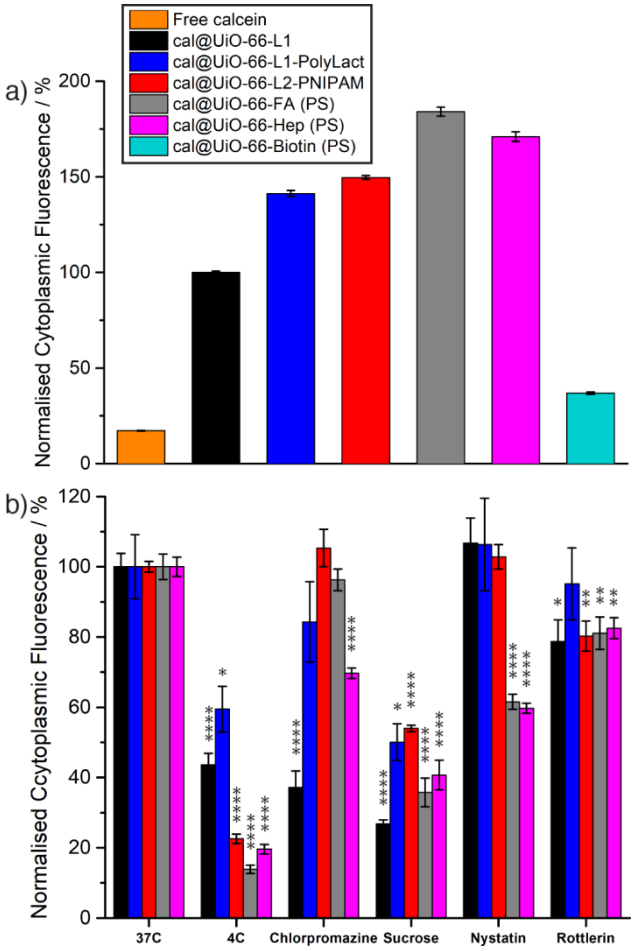

Figure 5. a) Endocytosis efficiencies of the calcein-loaded MOFs compared to calcein alone. b) Endocytosis efficiency of the calcein-loaded MOFs when incubated with various inhibitors. The Key from part a) applies in part b). The statistical significance was determined by ordinary one-way ANOVA and is indicated on the part b): * = P≤ 0.05 ** = P≤ 0.01 *** = P≤ 0.001 **** = P≤ 0.0001.

In general, cal@UiO-66 uptake is highly efficient compared to free calcein (6-10 fold increase), proving the validity of NMOFs as carriers to internalise cargo not able to efficiently cross the cell membrane by themselves. cal@UiO-66-Biot (PS) was, however, poorly internalised by HeLa cells compared to cal@UiO-66-L1, with the value of 37 ± 1% showing

that biotin coating might not be desirable to enhance NMOF cell internalisation. cal@UiO-66-FA (PS) had the highest internalisation, followed by cal@UiO-66-Hep (PS), cal@UiO-66-L2-PNIPAM, and cal@UiO-66-L1-Poly-Lact (Table 2). HeLa cells are known to over express the folate receptor (FR) on their surface,[47] and therefore the folate present on the surface of cal@UiO-66-FA (PS) could bind to the FR, providing a mode of targeting and enhanced internalisation of the NMOF by cells expressing FR.

To monitor the preferred routes of endocytosis, inhibitors were used to restrict uptake by certain pathways (SI, Section S6.3).[36] Chlorpromazine and sucrose were used to inhibit clathrin-mediated pathways although it is important to consider that sucrose can additionally inhibit some non-mediated endocytosis processes. Nystatin was used as an inhibitor of caveolae-mediated endocytosis and rottlerin was used to inhibit macropinocytosis. Both unfunctionalised cal@UiO-66[36] and cal@UiO-66-L1[32] have previously been shown to generally enter HeLa cells by clathrin-mediated endocytosis, while PEGylated cal@UiO-66-L1-PEG2000 showed caveolae-mediated endocytosis,[32] which is desirable for efficient treatment as the NMOF can potentially escape the early endosome, avoiding lysosome degradation and facilitating faster drug release in other cellular locations such as the cytosol.[48]

When cells were incubated at 4 °C in order to decrease energy-dependent processes, such as endocytosis, cell internalisation of the NMOFs decreased by 50-85% compared to the control at 37° C (Figure 5b). The only exception was cal@UiO-66-Biot (PS), where cell internalisation only decreased by 28%, confirming the observations from the previous uptake experiments that it is not efficiently internalised by HeLa cells (SI, Figure S66). As no efficient internalisation is observed, no further experiments were carried out with this sample. Folate receptors have been reported to often be located within caveolae invaginations;[47] cal@UiO-66-FA (PS) uptake decreased to 62 ± 2% when HeLa cells were incubated with nystatin, a well-known caveolae-mediated endocytosis inhibitor, while no inhibition was found when incubated with chlorpromazine (clathrin-mediated inhibitor) (96 ± 3%), and only a minor effect (81 ± 5%) was observed when rottlerin was inhibiting macropinocytosis pathways. Sucrose significantly decreased cal@UiO-66-FA (PS) uptake to 36 ± 4%, meaning that folate coating not only provides a way of cancer targeting, but also alters cancer cell endocytosis selection pathways from clathrin-mediated to both caveolae-mediated and non-mediated endocytosis. These results suggest that drug loaded UiO-66-FA samples have potential to be efficient therapeutic DDSs. Exposing HeLa cells to nystatin decreased cal@UiO-66-Hep (PS) cell internalisation to values of 60 ± 1%, showing that the heparin coated MOF is also partially internalised by caveolae-mediated endocytosis. However, in contrast to cal@UiO-66-FA (PS), clathrin-mediated routes also play a role in

HeLa cell internalisation of cal@UiO-66-Hep (PS), as normalised cell cytoplasmic fluorescence decreases to values of 70 ± 2%, while inhibiting macropinocytosis decreases the MOF normalised uptake to 83 ± 3%. Additionally, sucrose also decreased its cell internalisation to values of 41 ± 4%.

In the cases of cal@UiO-66-L1-PolyLact and cal@UiO-66-L2-PNIPAM, cell internalisation decreased when inhibiting with sucrose (50 ± 5% and 54 ± 1%, respectively), while no significant decrease was found when inhibiting clathrin-mediated (84 ± 11% and 105 ± 5% respectively) or caveolae-mediated routes (106 ± 13% and 103 ± 4% respectively), and only minor macropinocytosis attributions upon PNIPAM coating (80 ± 4%). These results indicate that these polymer-coated samples are mainly internalised by non-mediated endocytosis processes, with a significant contribution for cal@UiO-66-L1-PolyLact from energy independent processes.

Selectivity of Cytotoxicity of DCA-Loaded, Surface-Functionalised NMOFs

We previously reported the validity of the coordination modulation protocol to introduce a small molecule with high metabolic anticancer activity, dichloroacetate (DCA),[49,50] as a modulator that is attached to UiO-66 metal nodes during synthesis.[32] DCA is a pyruvate dehydrogenase kinase (PDK) inhibitor which has been investigated for over 25 years for the treatment of mitochondrial disorders such as lactic acidosis.[51] PDK is one of the main enzymes responsible for promoting glycolysis over glucose oxidation in cancer cells, as it can inhibit pyruvate dehydrogenase (PDH), an enzyme that converts pyruvate to acetylCoA.[52] Once glucose has been transformed to pyruvate, instead of being decarboxylated to form acetylCoA and entering the Krebs cycle in the mitochondria, pyruvate is alternatively transformed to lactate in the cytosol of cancer cells,[53] allowing them to grow in hypoxic conditions (low presence of oxygen) and resist apoptosis.[54] DCA shifts cancer cells metabolism from glycolysis back to glucose oxidation by PDH re-activation, decreasing the mitochondrial membrane hyperpolarisation and activating Kv channels, thus unlocking cancer cells from a state of apoptosis resistance without affecting growth of healthy cells.[49,50,55]

However, the hydrophilic nature of DCA means it does not efficiently cross the cell membrane[56] and thus free DCA displays low cytotoxicity, with IC_{50} values in the milimolar range, three orders of magnitude lower than anticancer drugs such as cisplatin.[57] DCA is rapidly cleared out from the blood stream, with initial half-life times of about an hour,[58] leading to poor efficacy and targeting when the drug is injected alone.[55,57] Nevertheless, cancer cells have shown remarkably lower resistance factors to DCA compared to cisplatin and other anticancer therapeutics,[57] which is a notable drawback for anticancer therapy.

Although DCA is not currently under clinical use as an anticancer drug, it has been studied as a potential metabolic cancer therapy since 2007,[49] with several clinical trials showing significant tumour remission without healthy cells damage, low side effects and toxicity, and safe chronic use.[59] However, due to its ability to cross the brain membrane barrier, chronic exposure to very high DCA doses can result in reversible peripheral neuropathy.[51]

We have chosen DCA as the object of our study due to the fact that its cytotoxic effect will only be observed if MOFs are able to deliver cargo into the cytosol and subsequently reach the mitochondria. This allows experimental confirmation that therapeutically active DCA-loaded MOF nanoparticles have been successfully internalised, and by specific endocytosis mechanisms that result in the DDS being localised in the cytosol rather than lysosomes. As such, DCA is an excellent mechanistic probe for the therapeutic efficiency and cellular internalisation of NMOFs,[32] while its less problematic side-effects, together with the lower cancer cells resistance towards it, compared to other anticancer drugs, make it a potential therapeutic candidate if it can be efficiently delivered.

From the chemical point of view, the lower pK_a value (1.96) of dichloroacetic acid means considerable amounts can be attached to UiO-66 Zr positions at defect sites during synthesis (Scheme 2), even in the presence of other functionalised modulators. Additionally, this concept of defect loading of drugs that act as modulators in synthesis could be applied to any therapeutic molecule containing carboxylate groups, such as doxorubicin.

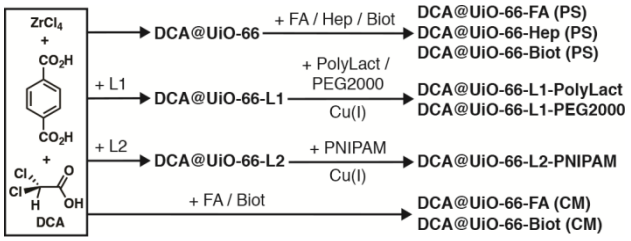

Scheme 2. Synthesis of DCA-loaded, surface modified MOFs obtained through coordination modulation (CM), click modulation, and postsynthetic exchange (PS).

Attaching a small molecule with anticancer activity to UiO-66 Zr positions during synthesis, creating defective structures, also allows the possibility of introducing a second drug into the MOF pores for multimodal treatments. For example, cisplatin prodrugs containing axial DCA ligands have been reported to be more effective than cisplatin, and able to overcome cisplatin resistance.[57] Similarly, DCA is known to enhance the anticancer effect of 5-fluorouracil (5-FU) and to reduce resistance.[60]

DCA@UiO-66, DCA@UiO-66-L1, and DCA@UiO-66-L2 were prepared (SI, Section S7.1) and found to be highly crystalline and phase pure, as determined by PXRD, with high DCA

content, 15-20% (*w/w*), measured by both TGA and inductively coupled plasma mass spectrometry (ICP-MS) analysis (Table 1). ^{1}H NMR spectroscopy showed incorporation of functionalised modulators incorporation (between 3 and 6 mol % compared to bdc) as well as DCA. Further characterisation of the samples' porosity showed that DCA is not stored in the pores, but attached to UiO-66 available zirconium positions, inducing defects and yielding highly porous nanoparticles of 70-170 nm in size, with BET areas between 1300 m^2g^{-1} and 1540 m^2g^{-1}, higher than unmodulated UiO-66.[41] In concordance, TGA profiles showed that DCA thermal decomposition occurs at a higher temperature than the one reported for the free drug,[61] and FT-IR profiles show shifting of the DCA carbonyl vibration band as a consequence of DCA coordination to available zirconium positions through its carboxylic acid group. During the preparation of this manuscript it was reported that the pK_a of the modulator also affects the colloidal stability of MOFs, with the authors finding better colloidal dispersion for MOFs synthesised using modulators with lower pK_a, as a consequence of the formation of defects and subsequent modulator incorporation.[62] Our own DCA-loaded samples were also found by DLS to be essentially monodisperse in water (SI, Figure S7.8).

The use of folic acid or biotin with DCA as a co-modulator was also studied (SI, Scheme S2) to successfully introduce both a metabolically active anticancer molecule and more complex surface functionalities to UiO-66 structure in only one synthetic step (SI, Section S7.2). As with the above DCA@NMOFs, full characterisation of the samples through PXRD, ^{1}H NMR spectroscopy, ICP-MS, FT-IR, TGA, SEM and nitrogen adsorption isotherms showed phase pure crystalline samples, with high DCA content (around 19% *w/w*, Table 1), functionalised modulator incorporation and appropriate size for drug delivery. The incorporation of both DCA and folic acid can also be tuned by changing the ratio of modulators (FA and DCA) introduced during synthesis. The samples were named as DCA_{10}@UiO-66-$FA_{0.25}$ (CM), DCA_5@UiO-66-FA_1 (CM), where the different numbers correlate to the equivalents of modulator added during synthesis, and DCA@UiO-66-Biot (CM).

Covalent attachment of the drug at defect sites throughout the MOF nanoparticle should facilitate slow release and the potential to overcome burst release, which can hinder many MOF-based DDSs, as well as allow the possibility of loading a second drug into the enhanced porosity for combined treatments. Importantly, the attachment of DCA throughout the MOF ensures it is not lost on postsynthetic modification. CuAAC covalent modifications yielded DCA@UiO-66-L1-PolyLact and DCA@UiO-66-L2-PNIPAM as we previously demonstrated for DCA@UiO-66-L1-PEG2000 (SI, Scheme S2), and full characterisation showed retention of crystallinity, polymer attachment and significant DCA content (SI, Section 7.3). Folic acid, biotin and heparin were also postsynthetically coordinated to

DCA@UiO-66 surface, yielding DCA@UiO-66-FA (PS), DCA@UiO-66-Biot (PS) and UiO-66-Hep (PS) while conserving DCA attachment. The DCA content of all samples, determined independently by TGA and ICP-MS, is given in Table 3.

Table 3. Particle sizes, determined by SEM, and DCA loadings, determined independently by TGA and ICP-MS, of the surface modified MOFs.

Sample	SEM Particle Size (nm)	DCA (TGA, % *w/w*)	DCA (ICP-MS, % *w/w*)
DCA@UiO-66	77 ± 24	17.0	16.9
DCA@UiO-66-L1	100 ± 15	15.9	15.5
DCA@UiO-66-L2	77 ± 11	18.7	18.9
DCA@UiO-66-L1-PolyLact	138 ± 27	9.0	7.6
DCA@UiO-66-L2-PNIPAM	159 ± 21	n/a[a]	3.2
DCA@UiO-66-FA (PS)	146 ± 38	15.8	13.3
DCA@UiO-66-Biot (PS)	130 ± 33	15.6	9.4
DCA@UiO-66-Hep (PS)	133 ± 33	n/a[a]	5.1
DCA_{10}@UiO-66-$FA_{0.25}$ (CM)	158 ± 23	19.6	18.9
DCA_5@UiO-66-FA_1 (CM)	91 ± 29	12.1	11.8
DCA@UiO-66-Biot (CM)	166 ± 22	19.0	20.7

[a]Could not be calculated due to overlapping thermal decomposition events.

To investigate the consequences of surface coating on the therapeutic efficacy of the surface functionalised NMOFs, the cytotoxicity of the materials against three different cell lines – HeLa (cervical cancer), MCF-7 (breast carcinoma) and HEK293 (healthy kidney) – was analysed by the MTS assay (SI, Section S8). At first, HeLa cell proliferation when incubated with the empty surface functionalised NMOFs for 72 h was investigated, finding that only UiO-66-L2-PNIPAM was cytotoxic for concentrations above 0.25 $mgmL^{-1}$, while incubation with other coated UiO-66 samples enhanced HeLa cells proliferation with a dose-response pattern, presumably as a consequence of the incorporation of the NMOFs' organic components into their metabolic cycle (SI, Section S8.1).

In order to study the therapeutic efficacies of the folate coated NMOFs and assess the different methods of surface modification, we incubated HeLa cells with various concentrations of DCA@UiO-66-FA (PS), DCA_{10}@UiO-66-$FA_{0.25}$ (CM) or DCA_5@UiO-66-FA_1 (CM) for 72 h. Figure 6 shows the HeLa cell viability for the different NMOFs, normalized with an untreated control. We have previously shown that empty UiO-66 is not cytotoxic towards HeLa cells,[33] and although unfunctionalised DCA@UiO-66 also does not decrease

HeLa cell proliferation (128 ± 5% cell viability at a concentration of 1 mgmL^{-1}), likely as a consequence of inefficient cytosolic release after clathrin-mediated internalisation, all the folate-coated, DCA-loaded MOFs had decreased proliferation to a certain extent in a dose responsive manner (Figure 6a). Interestingly, the postsynthetically coated DCA@UiO-66-FA (PS) was the least cytotoxic, with 74 ± 4% cell viability at a NMOF concentration of 1 mgmL^{-1}. Of the two samples prepared through coordination modulation, DCA_5@UiO-66-FA_1 (CM), which has a higher folate content, was the most cytotoxic, with 14 ± 6% of cell proliferation at a NMOF concentration of 0.25 mgmL^{-1} and killing all cells (2 ± 1%) when incubated with 1 mgmL^{-1} of NMOF in growth media. DCA_{10}@UiO-66-$FA_{0.25}$ (CM) started to reduce cell proliferation at 0.75 mgmL^{-1} (85 ± 3%) and only kills 52 ± 5% of cells at 1 mgmL^{-1}, despite containing more DCA (~19% *w/w*) than DCA_5@UiO-66-FA_1 (CM) (~12% *w/w*). Clearly the mode of external surface attachment of folate is key to therapeutic activity: the most cytotoxic folate-coated MOF has the lowest drug content. The enhanced cytotoxicity may be due to folate coating enhancing endocytosis efficiency and promoting caveolae-mediated endocytosis, which we showed previously enhanced cytotoxicity of PEGylated UiO-66 loaded with DCA.[32] The postsynthetically coated MOF will have the bulk of the folic acid on the nanoparticle external surface, while the NMOFs prepared by coordination modulation may have folate throughout the nanoparticles in defect sites, enhancing the targeting properties even after the onset of degradation. Cytotoxicity of free DCA towards HeLa was found to be negligible until cells were incubated with concentrations >4 mgmL^{-1}(SI, Section S8.3) confirming that effective delivery of DCA into cells by the DDSs is occurring, with a greater than 300 fold enhancement in cytotoxicity compared to the free drug when DCA is transported into HeLa cells by DCA_5@UiO-66-FA_1 (CM).

Interestingly, DCA@UiO-66-L1-PolyLact produced a similar effect on HeLa cell growth regardless of the incubation time, which could be indicative of its significant internalisation by energy-independent endocytosis, while empty UiO-66-L1-PolyLact did not show any toxicity. Inhibition of cell growth starts to be observed when incubated with 0.75 mgmL^{-1} of DCA-loaded MOF for 72 h (85 ± 3% cell viability), while it kills almost all HeLa cells at 1 mgmL^{-1} (Figure 6b). Although the empty UiO-66-L2-PNIPAM was already found to be cytotoxic at concentrations of 0.5 mgmL^{-1} and above, DCA loading enhanced its cytotoxic effects, with DCA@UiO-66-L2-PNIPAM killing all HeLa cells at the NMOF concentration of 0.25 mgmL^{-1}.

In contrast to folate coated NMOFs, although heparin coating resulted in enhanced endocytosis efficiency and partial uptake by caveolae-mediated endocytosis, no decrease in cell proliferation was found when HeLa cells were incubated with DCA@UiO-66-Hep for 72 h (Figure 6c). UiO-66-Hep showed undesirable degradation kinetics and colloidal stability when compared to UiO-66 precursor samples, and so may not be suitably stable.

Additionally, the growth of three different colon cancer cell lines has been reported to be stimulated upon heparin addition,[63] which might explain why, even if endocytosis efficiency and routes are enhanced, no anticancer efficacy is found in this case. In addition, no cytotoxicity was observed for DCA@UiO-66-Biot (PS) or DCA@UiO-66-Biot (CM) over 72 h of incubation, in concordance with the fact that endocytosis studies showed that cal@UiO-66-Biot (PS) is not efficiently taken up by HeLa cells.

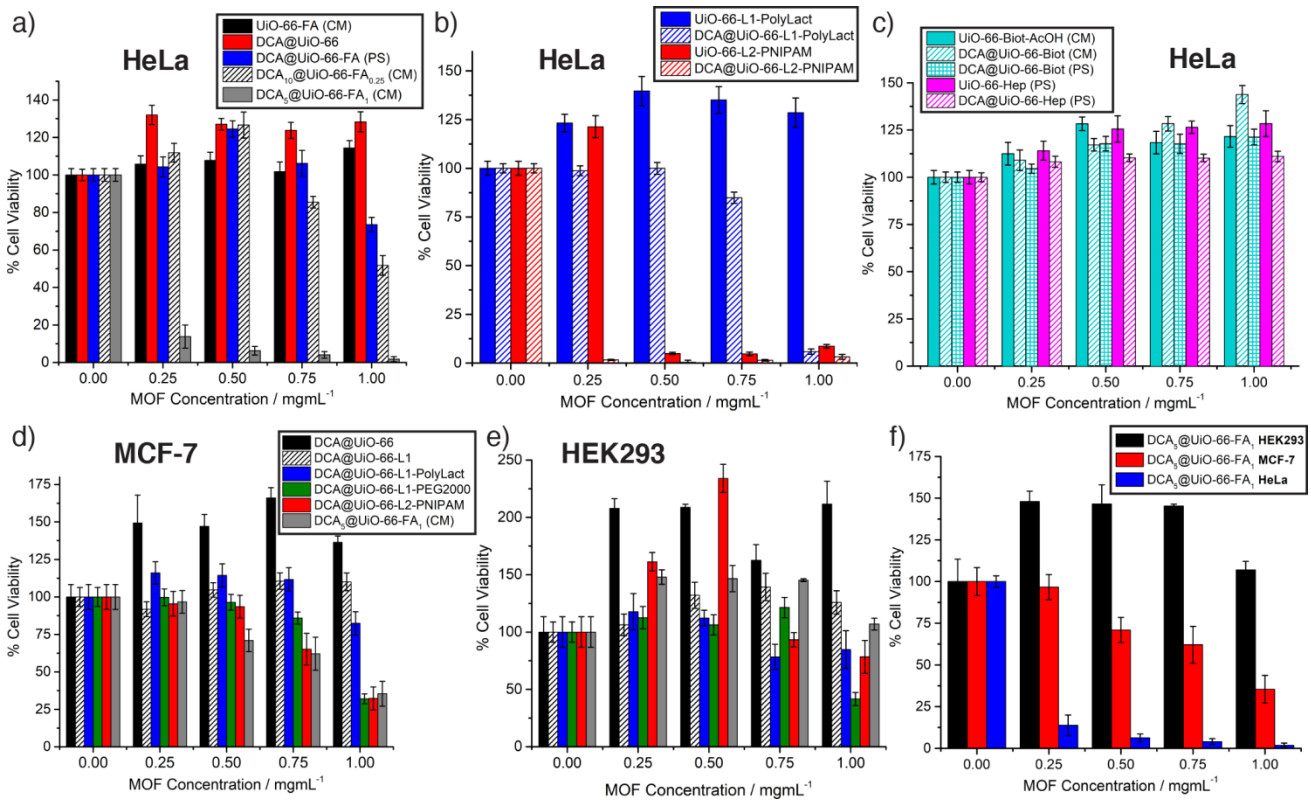

Figure 6. Cytotoxicity of UiO-66 samples as measured by MTS assay after 72 h incubation with the respective cells. a) HeLa cytotoxicity of the DCA-loaded, folic acid modified MOFs to assess the effect of surface functionalisation method. b) HeLa cytotoxicity of the "click modulated" MOFs, with and without DCA cargo. c) HeLa cytotoxicity of empty and DCA-loaded heparin and biotin modified samples. Cytotoxicities of the best DCA-loaded MOF candidates, as assessed by the HeLa experiments, for d) MCF-7 cells, and e) HEK293 cells (the key in part d applies to both). f) Comparison of cytotoxicity of DCA_5@UiO-66-FA_1 (CM) against the three cell-lines, indicating selective toxicity towards cancer cell lines only.

Because of these encouraging results, we further investigated the *in vitro* anticancer selectivity of the most cytotoxic candidates (DCA_5@UiO-66-FA_1 (CM), DCA@UiO-66-L1-PolyLact and UiO-66-L2-PNIPAM), by MTS assay (72 h incubation) against a breast cancer cell line (MCF-7, standing for Michigan Cancer Foundation-7), and a healthy kidney cell line

(HEK293, standing for human embryonic kidney cells 293). We compared the cell viability with the DCA-loaded, unfunctionalised NMOF, DCA@UiO-66 (SI, Section S8.2).[64]

We investigated the effect of the unfunctionalised DCA@UiO-66, which has the highest DCA content, against MCF-7 (Figure 6d) and HEK293 (Figure 6e) cells, finding no negative effects on their viability, with 136 ± 4% and 212 ± 20% cell proliferation after 72 h of incubation with a solution of 1 $mgml^{-1}$ of MOF compared to untreated controls. After 72 h of incubation, MCF-7 cell proliferation was drastically reduced when treated with DCA_5@UiO-66-FA_1 (CM) (Figure 6d). The dose-responsive curve showed a similar trend to the HeLa experiment, although with slightly lower efficacy; 71 ± 8% cell viability at a concentration of 0.5 $mgmL^{-1}$ and 35 ± 8% for a concentration of 1 $mgmL^{-1}$. More importantly, after 72 h of incubation with HEK293 cells, proliferation was not reduced in the presence of DCA_5@UiO-66-FA_1 (CM) at any concentration, with 107 ± 5% cell viability at the NMOF concentration of 1 $mgmL^{-1}$ (Figure 6e). These results suggest folate induces cancer cell-targeting, as HeLa cells have a higher FR overexpression than MCF-7,[65] and thus therapeutic efficacy in HeLa is more pronounced. On the other hand, HEK293 has been reported to have normal levels of expression of the FR,[66] and thus no effect is observed on their cell proliferation possibly as a consequence of poor internalisation and/or a lack of metabolic effect of DCA on healthy cells. It is also important to consider that free dichloroacetate was not cytotoxic to either MCF-7 or HEK293 cells at the concentrations delivered by the NMOFs (SI, Section S8.3), confirming the efficient delivery of DCA into the cells by the MOF DDSs.

Interestingly, DCA@UiO-66-L1-PolyLact and DCA@UiO-66-L2-PNIPAM were less cytotoxic towards MCF-7 and HEK293 than HeLa cells (Figures 6d and 6e). Incubation with DCA@UiO-66-L1-PolyLact for 72 h resulted in similar cytotoxicity values for both cell lines at higher concentrations; 82 ± 8% (MCF-7) and 85 ± 16% (HEK293) cell viability at 1 $mgml^{-1}$. DCA@UiO-66-L2-PNIPAM showed cytotoxicity for both, but more pronounced for MCF-7 (32 ± 8% viability) than for HEK293 (78 ± 14% viability) at 1 $mgmL^{-1}$. While the polymer coated, DCA loaded samples do show cytotoxicity towards MCF-7, the residual cytotoxicity towards HEK293 is a concern.

Our previous work with PEG-coated UiO-66 showed excellent cytotoxicity towards HeLa when loaded with DCA, and so the effect of polymer coating was further examined by determining the cytotoxicity of DCA@UiO-66-L1 and DCA@UiO-66-L1-PEG2000 towards MCF-7 and HEK293 cells. While DCA@UiO-66-L1 does not affect MCF-7 cell proliferation negatively, DCA@UiO-66-L1-PEG2000 induced some cytotoxicity with a 32 ± 3% cell proliferation during the same experiment, similar to the cell viability reported for HeLa cells (50 ± 3%) at the same concentration.[32] However, some unwanted cytotoxicity of DCA@UiO-

66-L1-PEG2000 was observed against HEK293 (42 ± 6% viability) at the highest concentration of 1 mgml^{-1}, in contrast to DCA@UiO-66-L1.

***In vitro* Immune Response to DCA-Loaded NMOFs**

The immune response toward exogenous materials plays a crucial role in any treatment efficacy; DDSs will not be efficient if they are cleared out of the blood stream by macrophages, or if they stimulate/suppress immune response or induce tissue damage [2]. Cytotoxicity, uptake efficiency and reactive oxygen species (ROS) production by immune cells such as macrophages or lymphocytes are of great importance when considering the efficiency of a DDS, but, to the best of our knowledge, only few studies have assessed these issues with NMOFs to date.[14,23,67,68] Importantly, it can provide further insights into possible treatment efficiency without resorting to early stage animal testing.

The cytotoxicity of empty and DCA-loaded candidate NMOFs towards both macrophages (J774 cell line) and a pool of peripheral blood lymphocytes (PBLs) isolated from the blood of three human donors were investigated (SI, Section S9). It has been reported that DCA does not affect the mitochondrial functions of healthy cells,[55] and therefore should not induce any cytotoxicity. Internalisation efficiency of the NMOFs by macrophage cells was investigated by incubation of J774 cells with 0.25 mgmL^{-1} of calcein loaded NMOFs, followed by analysis of intracellular fluorescence by FACS (SI, Section S9.1). Normalised cell fluorescence showed that only PEGylation decreased macrophage uptake, to levels of 80 ± 4% compared to UiO-66-L1. cal@UiO-66-FA (PS) was the most efficiently internalised NMOF, with a 189 ± 15% – expected, as activated macrophages are known to overexpress the folate receptor – followed by cal@UiO-66-L2-PNIPAM with a 176 ± 9% cell internalisation and cal@UiO-66-L1-PolyLact with a 155 ± 7% macrophage uptake efficiency.

MTT assays were carried out to assess the viability of J774 macrophage cells (Figure 7a) after incubation with several concentrations of surface modified UiO-66 in media for 48 h (SI, Section S9.2). No cytotoxicity was observed when incubating J774 cells with either UiO-66-FA (CM) or DCA_5@UiO-66-FA_1 (CM), despite the fact that, in contrast to the folate receptor negative HEK293 healthy cell line, activated macrophages overexpress the folate receptor.[69] In fact, cell proliferation was slightly enhanced (128 ± 10% and 142 ± 11%, respectively) at a NMOF concentration of 0.5 mgmL^{-1}. Similar results were obtained when a pool of PBLs was incubated with folate-coated NMOFs for 72 h, obtaining enhanced, dose-responsive cell proliferation by MTT assay for two independent experiments (one is plotted in Figure 7b, comparison available in SI) which showed similar trends. Viabilities of 295 ± 24% and 199 ± 34% for empty UiO-66-FA (CM) and 252 ± 28% and 146 ± 18% for DCA_5@UiO-66-FA_1 (CM) were found at 0.5 mgmL^{-1} incubation.

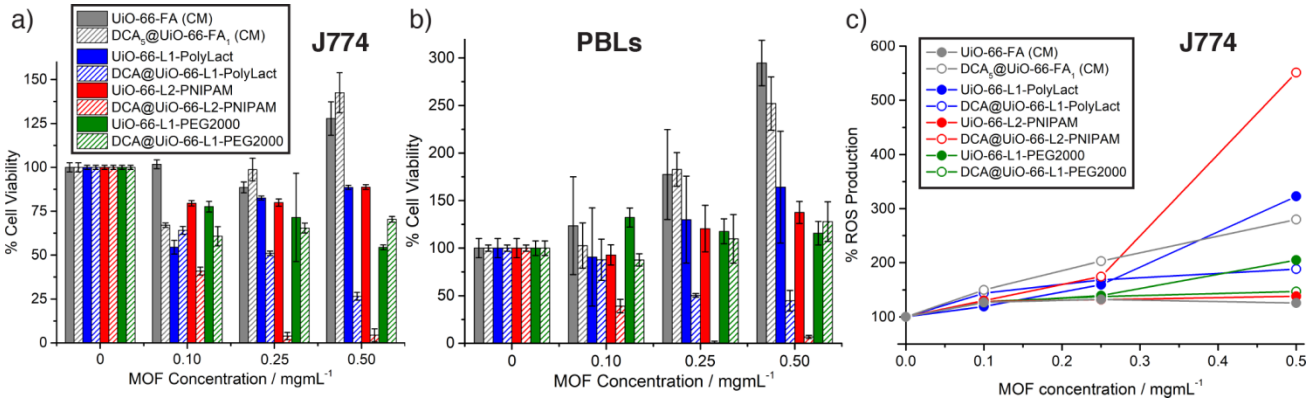

Figure 7. Cytotoxicity of empty and DCA-loaded UiO-66 samples against a) J774 macrophage cells and b) a pool of peripheral blood lymphocytes from three human donors. The key for part a) also applies in part b). c) Reactive oxygen species generation by J774 macrophage cells in the presence of empty and DCA-loaded UiO-66 samples.

Cytotoxicity assays showed that UiO-66-L1-PolyLact and UiO-66-L2-PNIPAM were well tolerated by J774 macrophages (both having 89 ± 1% cell viability at 0.5 mgmL^{-1}), although DCA@UiO-66-L1-PolyLact and DCA@UiO-66-L2-PNIPAM killed almost all cells, despite the reports that DCA does not affect healthy cells. Cell viability values of 27 ± 2% and 4 ± 4%, respectively, induced by incubation with 0.5 mgmL^{-1} NMOF (Figure 7a), suggest that the surface functionalities, together with DCA, might have some synergistic effect on metabolic activity. Similar results were observed for PBL cell proliferation (Figure 7b), for which the empty NMOFs, UiO-66-L1-PolyLact and UiO-66-L2-PNIPAM, did not induce cell death at 0.5 mgmL^{-1} (164 ± 59% and 134 ± 14% viability for the former; 138 ± 12% and 101 ± 41% viability for the latter), while incubation with DCA@UiO-66-L1-PolyLact and DCA@UiO-66-L2-PNIPAM under the same conditions reduced cell viability to values of 45 ± 11% and 17 ± 5% for the former, and 7 ± 2% and 3 ± 4% for the latter. These are major issues that may preclude the use of the polymer-coated samples *in vivo*.

The effect of the chemical constitution of the polymer chain was studied further by incubating J774 macrophages with our previously reported UiO-66-L1-PEG2000 and DCA@UiO-66-L1-PEG2000 materials, which decreased their cell proliferation to levels of 54 ± 1% and 70 ± 2%, respectively, at 0.5 mgmL^{-1} (Figure 7a). In contrast, UiO-66-L1-PEG2000 and DCA@UiO-66-L1-PEG2000 induced PBL cell proliferation from a single pool to levels of 116 ± 12% and 128 ± 21% compared to untreated cells at a concentration of 0.5 mgmL^{-1} (Figure 7b). Whilst the response of the J774 cells and the HEK293 cells to DCA@UiO-66-L1-PEG2000 could be problematic, the selectivity of the cytotoxicity of folate targeted, DCA loaded, DCA_5@UiO-66-FA_1 (CM) nanoparticles is very promising, killing almost all cancer cells whilst not negatively affecting the proliferation of healthy cells.

Reactive oxygen species (ROS) production was investigated to gain insights into the cytotoxic effects of the NMOFs and to assess induction of oxidative stress.[70] J774 macrophage cells and PBLs were incubated with different doses of the NMOFs over 2 h, followed by incubation with the intracellular fluorescent probe 2',7'-dichlorodihydrofluorescein diacetate (H2DC-FDA) in order to track ROS production by flow cytometry (SI, Section S9.3). DCA@UiO-66-L2-PNIPAM induced the highest ROS production in the J774 macrophages (Figure 7c), with a 5.5 fold increase at a NMOF concentration of 0.5 mg mL^{-1} a possible reason for the significant cytotoxicity, while the non-cytotoxic empty UiO-66-L2-PNIPAM only induced a 1.4 fold increase in ROS production at the same concentration. Whilst empty UiO-66-L1-PolyLact did not induce significant cytotoxicity in the J774 cell lines, higher ROS production was found when incubating macrophages with the empty sample (3.2 fold increase) compared to DCA@UiO-66-L1-PolyLact (1.9 fold increase), which is more cytotoxic. Similarly, incubating J774 macrophages with UiO-66-L1-PEG2000 induced a slightly higher ROS production (2 fold increase) than incubation with DCA@UiO-66-L1-PEG2000 (1.5 fold increase) for the same concentration. UiO-66-FA (CM) did not induce significant ROS production, with a 1.2 fold increase when incubating macrophages with a 0.5 $mgmL^{-1}$ concentration of NMOF, while DCA_5@UiO-66-FA_1 (CM) did induce ROS production with a 2.8 fold increase, although MTT assays showed cell proliferation was enhanced in all cases, suggesting that ROS production is not a major source of cytotoxicity for these particular MOFs. ROS production in PBLs was also monitored (SI, Section S9.3) with no discernible trends, although DCA_5@UiO-66-FA_1 was again well tolerated. These results suggest that while higher concentrations MOFs can induce some ROS production, it does not seem to result in cytotoxicity towards these healthy cells. It is also important to note that concentrations of DCA-loaded NMOFs lower than 0.5 $mgmL^{-1}$ did not induce considerable ROS production, despite being therapeutically active towards cancer cell lines.

CONCLUSIONS

In conclusion, we have assessed a number of different functionalities, as well as different surface modification protocols – coordination modulation, postsynthetic exchange, and covalent click modulation – for the surface functionalisation of UiO-66 nanoparticles for use in drug delivery. The use of carboxylate-containing drug molecules as modulators for synthesis of UiO-66 nanoparticles, in this study the anticancer metabolic target dichloroacetic acid, has been shown to be an efficient methodology to ensure high cargo loading at defect sites in one-pot syntheses that are also compatible with all the surface modification protocols. DCA modulation in particular generates colloidally-stable nanoparticles with high DCA-loading values that are amenable to further functionalisation without compromising porosity.

In nearly all cases, surface functionalisation enhances properties such as colloidal dispersion and stability towards phosphate-induced degradation compared to bare UiO-66. Internalisation by HeLa cells is enhanced – apart from biotin-coated samples – and certain surface coatings tune internalisation pathways to more desirable uptake routes, such as caveolae-mediated endocytosis, which may allow MOFs to escape the early endosome and result in increased cytosolic cargo release. Building on our preliminary results that show DCA@UiO-66-PEG2000 has enhanced cytotoxicity for HeLa as a consequence of its more efficient caveolae-mediated endocytosis, extensive *in vitro* studies of DCA-loaded materials have shown that folic acid coated MOFs exhibit selective cytotoxicity towards HeLa (cervical) and MCF-7 (breast cancer) cells, without adversely affecting proliferation of healthy kidney (HEK293), macrophage (J774) and PBL cells, possibly due to the over expression of the folate receptor on the surfaces of cancer cells and a preference for desirable caveolae-mediated endocytosis. The method of folic acid coating is vital – incorporation of folic acid and DCA in a one-pot, modulated synthesis produced significantly more active MOFs than postsynthetically coating MOFs with folic acid. Hence, the therapeutic efficiency of free DCA was drastically improved, with a >300 fold increase in selective cytotoxicity observed when loaded into DCA_5@UiO-66-FA_1 (CM), while uncoated DCA@UiO-66 did not produce any negative effect on the various cell lines.

The polymer-coated, DCA loaded MOFs prepared by click modulation also showed therapeutic potential, decreasing proliferation of the cancerous cell lines, but each had drawbacks. Both DCA@UiO-66-L1-PolyLact and DCA@UiO-66-L2-PNIPAM induced death in J774 macrophage cells and human lymphocytes – key components of the immune system – with the latter stimulating significant ROS production in J774 cells. While DCA@UiO-66-L1-PEG2000 was tolerated well by the immune system cells, as would be expected, it induced some cytotoxicity in healthy kidney cells at high concentrations, suggesting *in vivo* accumulation in healthy tissue might induce damage.

These results demonstrate the power of surface functionalisation and importance of cell internalisation pathways in the application of MOFs for drug delivery. The potential of DCA_5@UiO-66-FA_1 for use as a selective anticancer DDS for *in vivo* localised treatment is apparent, particularly given the use of the metabolic probe DCA as a modulator during synthesis resulting in a drug-loaded nanoparticle that is still porous and could be loaded with a second drug for synergistic multimodal therapy,[60] which we are currently investigating. The work also highlights the broad *in vitro* experimental toolkit available to provide information on cellular uptake, endocytosis mechanisms, immune response and cytotoxicity prior to any *in vivo* treatment, thus reducing the need for early stage animal testing and acting according to the three Rs: reduction, refinement and replacement.

ACKNOWLEDGEMENTS

RSF and DFJ thank the Royal Society for the receipt of University Research Fellowships. RSF and IAL thank the University of Glasgow for funding. This project received funding in part from the European Research Council (ERC) under the European Union's Horizon 2020 Programme for Research and Innovation (grant agreement no. 677289, SCoTMOF, ERC-2015-STG).

SUPPORTING INFORMATION

Synthetic procedures, full experimental characterisation of materials, drug loading protocols, stability assays, cytotoxicity assays.

REFERENCES

(1) Peer, D.; Karp, J. M.; Hong, S.; Farokhzad, O. C.; Margalit, R.; Langer, R. Nanocarriers as an Emerging Platform for Cancer Therapy. *Nat. Nanotechnol.* **2007**, *2*, 751-760.

(2) Dobrovolskaia, M. A.; McNeil, S. E. Immunological Properties of Engineered Nanomaterials. *Nat. Nanotechnol.* **2007**, *2*, 469-478.

(3) Huang, X.; Brazel, C. S. On the Importance and Mechanisms of Burst Release in Matrix-Controlled Drug Delivery Systems. *J. Control. Release* **2001**, *73*, 121-136.

(4) Sur, S.; Fries, A. C.; Kinzler, K. W.; Zhou, S.; Vogelstein, B. Remote Loading of Preencapsulated Drugs into Stealth Liposomes. *Proc. Natl. Acad. Sci. U. S. A.* **2014**, *111*, 2283-2288.

(5) Lewinski, N.; Colvin, V.; Drezek, R. Cytotoxicity of Nanoparticles *Small.* **2008**, *4*, 26-49.

(6) Iversen, T.-G.; Skotland, T.; Sandvig, K. Endocytosis and Intracellular Transport of Nanoparticles: Present Knowledge and Need for Future Studies. *Nano Today* **2011**, *6*, 176-185.

(7) Furukawa, H.; Cordova, K. E.; O'Keeffe, M.; Yaghi, O. M. The Chemistry and Applications of Metal-Organic Frameworks. *Science* **2013**, *341*, 1230444.

(8) Huxford, R. C.; Rocca, J. D.; Lin, W. Metal-Organic Frameworks as Potential Drug Carriers. *Curr. Opin. Chem. Biol.* **2010**, *14*, 262-268.

(9) Horcajada, P.; Gref, R.; Baati, T.; Allan, P. K.; Maurin, G.; Couvreur, P.; Férey, G.; Morris, R. E.; Serre, C. Metal–Organic Frameworks in Biomedicine. *Chem. Rev.* **2012**, *112*, 1232-1268.

(10) Horcajada, P.; Chalati, T.; Serre, C.; Gillet, B.; Sebrie, C.; Baati, T.; Eubank, J. F.; Heurtaux, D.; Clayette, P.; Kreuz, C.; Chang, J.-S.; Hwang, Y. K.; Marsaud, V.; Bories, P.-N.; Cynober, L.; Gil, S.; Ferey, G.; Couvreur, P.; Gref, R. Porous Metal-Organic Framework Nanoscale Carriers as a Potential Platform for Drug Delivery and Imaging. *Nat. Mater.* **2010**, *9*, 172-178.

(11) Bogart, L. K.; Pourroy, G.; Murphy, C. J.; Puntes, V.; Pellegrino, T.; Rosenblum, D.; Peer, D.; Levy, R. Nanoparticles for Imaging, Sensing, and Therapeutic Intervention. *ACS Nano* **2014**, *8*, 3107-3122.

(12) Yang, J.; Chen, X.; Li, Y.; Zhuang, Q.; Liu, P.; Gu, J. Zr-Based MOFs Shielded with Phospholipid Bilayers: Improved Biostability and Cell Uptake for Biological Applications. *Chem. Mater.* **2017**, *29*, 4580-4589.

(13) Gindy, M. E.; Prud'homme, R. K. Multifunctional Nanoparticles for Imaging, Delivery and Targeting in Cancer Therapy. *Expert Opin. Drug Deliv.* **2009**, *6*, 865-878.

(14) Bellido, E.; Hidalgo, T.; Lozano, M. V.; Guillevic, M.; Simón-Vázquez, R.; Santander-Ortega, M. J.; González-Fernández, Á.; Serre, C.; Alonso, M. J.; Horcajada, P. Heparin-Engineered Mesoporous Iron Metal-Organic Framework Nanoparticles: Toward Stealth Drug Nanocarriers. *Adv. Healthc. Mater.* **2015**, *4*, 1246-1257.

(15) Zheng, H.; Zhang, Y.; Liu, L.; Wan, W.; Guo, P.; Nyström, A. M.; Zou, X. One-pot Synthesis of Metal–Organic Frameworks with Encapsulated Target Molecules and Their Applications for Controlled Drug Delivery. *J. Am. Chem. Soc.* **2016**, *138*, 962-968.

(16) McGuire, C. V.; Forgan, R. S. The Surface Chemistry of Metal-Organic Frameworks. *Chem. Commun.* **2015**, *51*, 5199-5217.

(17) Rijnaarts, T.; Mejia-Ariza, R.; Egberink, R. J. M.; van Roosmalen, W.; Huskens, J. Metal–Organic Frameworks (MOFs) as Multivalent Materials: Size Control and Surface Functionalization by Monovalent Capping Ligands. *Chem. Eur. J.* **2015**, *21*, 10296-10301.

(18) Rowe, M. D.; Thamm, D. H.; Kraft, S. L.; Boyes, S. G. Polymer-Modified Gadolinium Metal-Organic Framework Nanoparticles Used as Multifunctional Nanomedicines for the Targeted Imaging and Treatment of Cancer. *Biomacromolecules* **2009**, *10*, 983-993.

(19) Röder, R.; Preiß, T.; Hirschle, P.; Steinborn, B.; Zimpel, A.; Höhn, M.; Rädler, J. O.; Bein, T.; Wagner, E.; Wuttke, S.; Lächelt, U. Multifunctional Nanoparticles by Coordinative

Self-Assembly of His-Tagged Units with Metal–Organic Frameworks. *J. Am. Chem. Soc.* **2017**, *139*, 2359-2368.
(20) Zimpel, A.; Preiß, T.; Röder, R.; Engelke, H.; Ingrisch, M.; Peller, M.; Rädler, J. O.; Wagner, E.; Bein, T.; Lächelt, U.; Wuttke, S. Imparting Functionality to MOF Nanoparticles by External Surface Selective Covalent Attachment of Polymers. *Chem. Mater.* **2016**, *28*, 3318-3326.
(21) Liu, S.; Zhai, L.; Li, C.; Li, Y.; Guo, X.; Zhao, Y.; Wu, C. Exploring and Exploiting Dynamic Noncovalent Chemistry for Effective Surface Modification of Nanoscale Metal-Organic Frameworks. *ACS Appl. Mater. Interfaces* **2014**, *6*, 5404-5412.
(22) Wang, S.; McGuirk, C. M.; Ross, M. B.; Wang, S.; Chen, P.; Xing, H.; Liu, Y.; Mirkin, C. A. General and Direct Method for Preparing Oligonucleotide-Functionalized Metal–Organic Framework Nanoparticles. *J. Am. Chem. Soc.* **2017**, *139*, 9827-9830.
(23) Wang, Z.; Fu, Y.; Kang, Z.; Liu, X.; Chen, N.; Wang, Q.; Tu, Y.; Wang, L.; Song, S.; Ling, D.; Song, H.; Kong, X.; Fan, C. Organelle-Specific Triggered Release of Immunostimulatory Oligonucleotides from Intrinsically Coordinated DNA–Metal–Organic Frameworks with Soluble Exoskeleton. *J. Am. Chem. Soc.* **2017**, *139*, 15784-15791.
(24) Kondo, M.; Furukawa, S.; Hirai, K.; Kitagawa, S. Coordinatively Immobilized Monolayers on Porous Coordination Polymer Crystals. *Angew. Chem. Int. Ed.* **2010**, *49*, 5327-5330.
(25) Rieter, W. J.; Pott, K. M.; Taylor, K. M. L.; Lin, W. Nanoscale Coordination Polymers for Platinum-Based Anticancer Drug Delivery. *J. Am. Chem. Soc.* **2008**, *130*, 11584-11585.
(26) Yu, Y.; Li, Y.; Wang, W.; Jin, M.; Du, Z.; Li, Y.; Duan, J.; Yu, Y.; Sun, Z. Acute Toxicity of Amorphous Silica Nanoparticles in Intravenously Exposed ICR Mice. *PLoS One* **2013**, *8*, e61346.
(27) Morris, W.; Briley, W. E.; Auyeung, E.; Cabezas, M. D.; Mirkin, C. A. Nucleic Acid–Metal Organic Framework (MOF) Nanoparticle Conjugates. *J. Am. Chem. Soc.* **2014**, *136*, 7261-7264.
(28) Taylor-Pashow, K. M. L.; Rocca, J. D.; Xie, Z.; Tran, S.; Lin, W. Post-Synthetic Modifications of Iron-Carboxylate Nanoscale Metal-Organic Frameworks for Imaging and Drug Delivery. *J. Am. Chem. Soc.* **2009**, *131*, 14261-14263.
(29) Jung, S.; Kim, Y.; Kim, S. J.; Kwon, T. H.; Huh, S.; Park, S. Bio-functionalization of Metal-Organic Frameworks by Covalent Protein Conjugation. *Chem. Commun.* **2011**, *47*, 2904-2906.
(30) Bai, Y.; Dou, Y.; Xie, L.-H.; Rutledge, W.; Li, J.-R.; Zhou, H.-C. Zr-based Metal-Organic Frameworks: Design, Synthesis, Structure, and Applications. *Chem. Soc. Rev.* **2016**, *45*, 2327-2367.
(31) He, C.; Lu, K.; Liu, D.; Lin, W. Nanoscale Metal–Organic Frameworks for the Co-Delivery of Cisplatin and Pooled siRNAs to Enhance Therapeutic Efficacy in Drug-Resistant Ovarian Cancer Cells. *J. Am. Chem. Soc.* **2014**, *136*, 5181-5184.
(32) Abánades Lázaro, I.; Haddad, S.; Sacca, S.; Orellana-Tavra, C.; Fairen-Jimenez, D.; Forgan, R. S. Selective Surface PEGylation of UiO-66 Nanoparticles for Enhanced Stability, Cell Uptake, and pH-Responsive Drug Delivery. *Chem* **2017**, *2*, 561-578.
(33) Orellana-Tavra, C.; Baxter, E. F.; Tian, T.; Bennett, T. D.; Slater, N. K. H.; Cheetham, A. K.; Fairen-Jimenez, D. Amorphous Metal-Organic Frameworks for Drug Delivery. *Chem. Commun.* **2015**, *51*, 13878-13881.
(34) Orellana-Tavra, C.; Haddad, S.; Marshall, R. J.; Abánades Lázaro, I.; Boix, G.; Imaz, I.; Maspoch, D.; Forgan, R. S.; Fairen-Jimenez, D. Tuning the Endocytosis Mechanism of Zr-Based MOFs Through Linker Functionalization. *ACS Appl. Mater. Interfaces* **2017**, *9*, 35516-35525.
(35) Orellana-Tavra, C.; Marshall, R. J.; Baxter, E. F.; Lazaro, I. A.; Tao, A.; Cheetham, A. K.; Forgan, R. S.; Fairen-Jimenez, D. Drug Delivery and Controlled Release from Biocompatible Metal-Organic Frameworks using Mechanical Amorphization. *J. Mater. Chem. B* **2016**, *4*, 7697-7707.

(36) Orellana-Tavra, C.; Mercado, S. A.; Fairen-Jimenez, D. Endocytosis Mechanism of Nano Metal-Organic Frameworks for Drug Delivery. *Adv. Healthc. Mater.* **2016**, *5*, 2261-2270.
(37) Zhu, X.; Gu, J.; Wang, Y.; Li, B.; Li, Y.; Zhao, W.; Shi, J. Inherent Anchorages in UiO-66 Nanoparticles for Efficient Capture of Alendronate and its Mediated Release. *Chem. Commun.* **2014**, *50*, 8779-8782.
(38) Tan, L.-L.; Li, H.; Zhou, Y.; Zhang, Y.; Feng, X.; Wang, B.; Yang, Y.-W. Zn^{2+}-Triggered Drug Release from Biocompatible Zirconium MOFs Equipped with Supramolecular Gates. *Small* **2015**, *11*, 3807-3813.
(39) Teplensky, M. H.; Fantham, M.; Li, P.; Wang, T. C.; Mehta, J. P.; Young, L. J.; Moghadam, P. Z.; Hupp, J. T.; Farha, O. K.; Kaminski, C. F.; Fairen-Jimenez, D. Temperature Treatment of Highly Porous Zirconium-Containing Metal–Organic Frameworks Extends Drug Delivery Release. *J. Am. Chem. Soc.* **2017**, *139*, 7522-7532.
(40) Chen, D.; Yang, D.; Dougherty, C. A.; Lu, W.; Wu, H.; He, X.; Cai, T.; Van Dort, M. E.; Ross, B. D.; Hong, H. In Vivo Targeting and Positron Emission Tomography Imaging of Tumor with Intrinsically Radioactive Metal–Organic Frameworks Nanomaterials. *ACS Nano* **2017**, *11*, 4315-4327.
(41) Cavka, J. H.; Jakobsen, S.; Olsbye, U.; Guillou, N.; Lamberti, C.; Bordiga, S.; Lillerud, K. P. A New Zirconium Inorganic Building Brick Forming Metal Organic Frameworks with Exceptional Stability. *J. Am. Chem. Soc.* **2008**, *130*, 13850-13851.
(42) Trickett, C. A.; Gagnon, K. J.; Lee, S.; Gándara, F.; Bürgi, H.-B.; Yaghi, O. M. Definitive Molecular Level Characterization of Defects in UiO-66 Crystals. *Angew. Chem. Int. Ed.* **2015**, *54*, 11162-11167.
(43) Nagata, S.; Kokado, K.; Sada, K. Metal-Organic Framework Tethering PNIPAM for ON-OFF Controlled Release in Solution. *Chem. Commun.* **2015**, *51*, 8614-8617.
(44) Hermes, S.; Witte, T.; Hikov, T.; Zacher, D.; Bahnmüller, S.; Langstein, G.; Huber, K.; Fischer, R. A. Trapping Metal-Organic Framework Nanocrystals: An in-Situ Time-Resolved Light Scattering Study on the Crystal Growth of MOF-5 in Solution. *J. Am. Chem. Soc.* **2007**, *129*, 5324-5325.
(45) Guo, H.; Zhu, Y.; Wang, S.; Su, S.; Zhou, L.; Zhang, H. Combining Coordination Modulation with Acid–Base Adjustment for the Control over Size of Metal–Organic Frameworks. *Chem. Mater.* **2012**, *24*, 444-450.
(46) Bellido, E.; Guillevic, M.; Hidalgo, T.; Santander-Ortega, M. J.; Serre, C.; Horcajada, P. Understanding the Colloidal Stability of the Mesoporous MIL-100(Fe) Nanoparticles in Physiological Media. *Langmuir* **2014**, *30*, 5911-5920.
(47) Zwicke, G. L.; Mansoori, G. A.; Jeffery, C. J. Utilizing the Folate Receptor for Active Targeting of Cancer Nanotherapeutics. *Nano Rev.* **2012**, *3*, 18496.
(48) Kiss, A. L.; Botos, E. Endocytosis via Caveolae: Alternative Pathway with Distinct Cellular Compartments to Avoid Lysosomal Degradation? *J. Cell. Mol. Med.* **2009**, *13*, 1228-1237.
(49) Bonnet, S.; Archer, S. L.; Allalunis-Turner, J.; Haromy, A.; Beaulieu, C.; Thompson, R.; Lee, C. T.; Lopaschuk, G. D.; Puttagunta, L.; Bonnet, S.; Harry, G.; Hashimoto, K.; Porter, C. J.; Andrade, M. A.; Thebaud, B.; Michelakis, E. D. A Mitochondria-K+ Channel Axis Is Suppressed in Cancer and Its Normalization Promotes Apoptosis and Inhibits Cancer Growth. *Cancer Cell* **2007**, *11*, 37-51.
(50) Michelakis, E. D.; Webster, L.; Mackey, J. R. Dichloroacetate (DCA) as a Potential Metabolic-Targeting Therapy for Cancer. *Br. J. Cancer* **2008**, *99*, 989-994.
(51) Stacpoole, P. W.; Henderson, G. N.; Yan, Z.; James, M. O. Clinical Pharmacology and Toxicology of Dichloroacetate. *Environ. Health Perspect.* **1998**, *106*, 989-994.
(52) Kim, J.-W.; Tchernyshyov, I.; Semenza, G. L.; Dang, C. V. HIF-1-Mediated Expression of Pyruvate Dehydrogenase Kinase: A Metabolic Switch Required for Cellular Adaptation to Hypoxia. *Cell Metab.* **2006**, *3*, 177-185.
(53) Favier, J.; Brière, J.-J.; Burnichon, N.; Rivière, J.; Vescovo, L.; Benit, P.; Giscos-Douriez, I.; De Reyniès, A.; Bertherat, J.; Badoual, C.; Tissier, F.; Amar, L.; Libé, R.; Plouin,

P.-F.; Jeunemaitre, X.; Rustin, P.; Gimenez-Roqueplo, A.-P. The Warburg Effect Is Genetically Determined in Inherited Pheochromocytomas. *PLoS One* **2009**, *4*, e7094.
(54) Cairns, R. A.; Harris, I. S.; Mak, T. W. Regulation of Cancer Cell Metabolism. *Nat. Rev. Cancer* **2011**, *11*, 85-95.
(55) Wong, J. Y.; Huggins, G. S.; Debidda, M.; Munshi, N. C.; De Vivo, I. Dichloroacetate Induces Apoptosis in Endometrial Cancer Cells. *Gynecol. Oncol.* **2008**, *109*, 394-402.
(56) Trapella, C.; Voltan, R.; Melloni, E.; Tisato, V.; Celeghini, C.; Bianco, S.; Fantinati, A.; Salvadori, S.; Guerrini, R.; Secchiero, P.; Zauli, G. Design, Synthesis, and Biological Characterization of Novel Mitochondria Targeted Dichloroacetate-Loaded Compounds with Antileukemic Activity. *J. Med. Chem.* **2016**, *59*, 147-156.
(57) Zajac, J.; Kostrhunova, H.; Novohradsky, V.; Vrana, O.; Raveendran, R.; Gibson, D.; Kasparkova, J.; Brabec, V. Potentiation of Mitochondrial Dysfunction in Tumor Cells by Conjugates of Metabolic Modulator Dichloroacetate with a Pt(IV) Derivative of Oxaliplatin. *J. Inorg. Biochem.* **2016**, *156*, 89-97.
(58) Stacpoole, P. W.; Nagaraja, N. V.; Hutson, A. D. Efficacy of Dichloroacetate as a Lactate-Lowering Drug. *J. Clin. Pharmacol.* **2003**, *43*, 683-691.
(59) Khan, A.; Andrews, D.; Shainhouse, J.; Blackburn, A. C. Long-term Stabilization of Metastatic Melanoma with Sodium Dichloroacetate. *World J. Clin. Oncol.* **2017**, *8*, 371-377.
(60) Xuan, Y.; Hur, H.; Ham, I.-H.; Yun, J.; Lee, J.-Y.; Shim, W.; Kim, Y. B.; Lee, G.; Han, S.-U.; Cho, Y. K. Dichloroacetate attenuates hypoxia-induced resistance to 5-fluorouracil in gastric cancer through the regulation of glucose metabolism *Exp. Cell Res.* **2014**, *321*, 219-230.
(61) Lide, D. R. CRC Handbook of Chemistry and Physics 86TH Edition. *CRC Press, Taylor & Francis, Boca Raton,* **2005**, 3-150.
(62) Morris, W.; Wang, S.; Cho, D.; Auyeung, E.; Li, P.; Farha, O. K.; Mirkin, C. A. Role of Modulators in Controlling the Colloidal Stability and Polydispersity of the UiO-66 Metal–Organic Framework. *ACS Appl. Mater. Interfaces* **2017**, *9*, 33413-33418.
(63) Chatzinikolaou, G.; Nikitovic, D.; Asimakopoulou, A.; Tsatsakis, A.; Karamanos, N. K.; Tzanakakis, G. N. Heparin—A Unique Stimulator of Human Colon Cancer Cells' Growth. *IUBMB Life* **2008**, *60*, 333-340.
(64) During the experiments, it was noted that the standard HeLa experimental procedure – washing the cells three times with PBS to remove unabsorbed NMOF – resulted in loss of cells, presumably due to poor adhesion to the well plate. To avoid the risk of overestimating cytotoxicity, the protocol was amended to contain only one PBS wash. The results below follow this single wash protocol, but a full comparison with the standard three wash protocol is given in the Supporting Information, Figure S98, where the trends are similar but the absolute values differ slightly.
(65) Sudimack, J.; Lee, R. J. Targeted Drug Delivery via the Folate Receptor. *Adv. Drug Deliv. Rev.* **2000**, *41*, 147-162.
(66) Chen, C.; Ke, J.; Zhou, X. E.; Yi, W.; Brunzelle, J. S.; Li, J.; Yong, E.-L.; Xu, H. E.; Melcher, K. Structural Basis for Molecular Recognition of Folic Acid by Folate Receptors. *Nature* **2013**, *500*, 486-489.
(67) Lu, K.; He, C.; Lin, W. A Chlorin-Based Nanoscale Metal–Organic Framework for Photodynamic Therapy of Colon Cancers. *J. Am. Chem. Soc.* **2015**, *137*, 7600-7603.
(68) Zhang, Y.; Liu, C.; Wang, F.; Liu, Z.; Ren, J.; Qu, X. Metal-Organic-Framework-Supported Immunostimulatory Oligonucleotides for Enhanced Immune Response and Imaging. *Chem. Commun.* **2017**, *53*, 1840-1843.
(69) Varghese, B.; Vlashi, E.; Xia, W.; Ayala Lopez, W.; Paulos, C. M.; Reddy, J.; Xu, L. C.; Low, P. S. Folate Receptor-Beta in Activated Macrophages: Ligand Binding and Receptor Recycling Kinetics. *Mol. Pharm.* **2014**, *11*, 3609-3616.
(70) Birben, E.; Sahiner, U. M.; Sackesen, C.; Erzurum, S.; Kalayci, O. Oxidative Stress and Antioxidant Defense. *World Allergy Organ. J.* **2012**, *5*, 9-19.